A combined experimental and numerical approach for radiation heat transfer in semi-crystalline thermoplastics

Sinan Boztepe, Olivier de Almeida, Rémi Gilblas, Yannick Le Maoult, Fabrice Schmidt, Christian Gerlach

A combined experimental and numerical approach for radiation heat transfer in semi-crystalline thermoplastics

Sinan Boztepe[a,*], Olivier de Almeida[a], Rémi Gilblas[a], Yannick Le Maoult[a], Fabrice Schmidt[a], Christian Gerlach[b]

[a] Université de Toulouse, IMT Mines Albi, ICA (Institut Clément Ader), Campus Jarlard, F-81013, Albi cedex 09, France
[b] Procter & Gamble, Brussels Innovation Center (BIC), Temselaan 100, 1853, Strombeek Bever, Belgium

A B S T R A C T

This paper proposes a novel experimental-numerical approach for radiation heat transfer in semi-crystalline thermoplastics. The proposed experimental and numerical approaches were analyzed here for the case of IR heating of linear polyethylene (PE). The challenges for radiation transport in semi-crystalline polymers may be categorized into the two main aspects: optical heterogeneity in polymer medium due to semi-crystalline nature and, semi-transparency in certain type of such polymers, like PE. In this study, we address the temperature dependence in the thermo-optical properties of semi-crystalline thermoplastics concerning its effect as a thermal radiation parameter for radiation heat transfer modeling of such type of polymers. The temperature dependence in the optical properties of PE, namely transmittance and reflectance characteristics, were experimentally analyzed under heating condition and, the temperature-dependent thermo-optical properties of PE was determined. The experimental analyses showed that the change in the thermo-optical properties under heating is related to change in the optical scattering behavior in PE medium since it is strongly affected by its crystalline structure. The radiation heat transfer model was built based on optically homogeneous medium assumption at which the change in the amount of radiative energy absorbed by the PE medium under heating was introduced without modeling how the light scatters inside of the medium. Thus, the effect of optical scattering on the absorption characteristics of PE under varying temperature was taken into account without modeling the spatial distribution of the scattered light intensity at microscopic level, which offers computationally cost-effective numerical solutions. The accuracy of the numerical model was analyzed performing IR heating experiments where IR thermography and thermocouples were employed for the surface temperature measurements. Due to the semi-transparent nature of PE, an experimental method was developed for IR thermography of PE and its accuracy was analyzed. The experimental-numerical comparisons showed that the temperature field on PE can be closely predicted using its temperature-dependent thermo-optical properties. Thanks to the adopted comparative case study, it was demonstrated how the temperature field predictions may deviate from the experimental thermal measurements due to the ignorance of this temperature dependence. Considering any type of monochromatic or polychromatic radiation source, the combined experimental-numerical approach proposed here may be adopted for temperature field predictions and non-invasive surface temperature measurements on the radiatively heated semi-crystalline thermoplastics.-

Keywords:
Radiation heat transfer modeling
Temperature-dependent thermo-optical properties
IR thermography
Polyethylene
Optical scattering

1. Introduction

IR heating is widely used for thermoforming process of semi-crystalline thermoplastics. Thermoforming window - which is the temperature range required for a successful forming process - of semi-crystalline thermoplastics is much narrower than amorphous thermoplastics, as the latter one is driven into rubber-like state above their glass transition temperature (T_g) that provides relatively large processing window [1]. Conversely, semi-crystalline thermoplastics can be softened enough around their melting range which causes a narrow thermoforming window. Above T_g of such a polymer, its semi-crystalline phase still stands that keeps the material in tough-elastic state until crystals melt down in melting range [1,2]. As a consequence, the final temperature state at the end of the heating stage plays a major role for achieving a successful forming process with respect to the quality of a thermoformed part. Therefore, predictive model for accurate

* Corresponding author.
E-mail address: sboztepe@mines-albi.fr (S. Boztepe).

temperature distributions is crucially important whereas it is known that the crystalline structure of polymers introduces an optically heterogeneous medium which causes optical scattering phenomenon [3–7].

In terms of modeling the radiation heat transfer in optically heterogeneous media, numerous examples of modeling approaches exist in literature that adopt well-known optical scattering theories, such as Rayleigh-Debye-Gans [8] or Mie [9,10] theory which allows to predict the spatial distribution of the scattered light intensity accurately. However, such radiation heat transfer models that handle complex radiation physics may be computationally costly, especially if spectral or geometrical complexity in a heated component is involved [11]. In contrast to laser heating applications, the radiation emitted by an IR source and transferred through a polymer medium is not monochromatic, but in a range, which introduces such a complexity in terms of modeling of optical scattering, as the scattering behavior may change under varying wavelength in the spectral range of emitted radiation. Such a wavelength-dependent scattering behavior in semi-crystalline polymers was discussed in Refs. [4,5,12]. The common point that was stressed out in those studies is that the scattering behavior becomes weaker considering an increase in the wavelengths roughly between 0.5 μm and 2 μm, which lies in the visible (VIS) and near-infrared (NIR) ranges.

Apart from the computational cost due to spectral complexity of IR radiation, the strong coupling between the crystalline structure of unfilled semi-crystalline thermoplastics and their optical scattering behavior may also increase the complexity of a numerical approach, and thus computational cost. It is known that optical scattering in semi-crystalline polymers are strongly related to their crystalline structure where the optical scattering behavior may evolve under heating, due to a potential change in their crystalline phase at the temperatures close to their melting ranges. It may therefore be useful to adopt a numerical model that considers this temperature-dependent optical behavior. Generally speaking, the studies that focus on the radiation heat transfer modeling for unfilled semi-crystalline thermoplastics rely on their thermo-optical properties analyzed at room temperature which results in a lack of modeling predictions in terms of temperature dependence in their absorption characteristics. One of the first efforts was given by Keller et al. [13] to explain temperature dependence in the absorption characteristics of various semi-crystalline polymers which was eventually used as numerical input for laser processing modeling. In their study, it was experimentally proven that the optical penetration depth of nylon 11 (PA 11), which physically represents how strong radiation energy attenuates into the medium, increases once the temperature increases while an inverse trend was observed for polyethylene terephthalate (PET). Becker et al. [14] proposed temperature-dependent optical properties for semi-crystalline polypropylene (PP), named as "*effective absorption constant*". However, the temperature dependency in absorption characteristics of PP was modeled based on the change in the density of the polymer in the corresponding temperature range, eluding the physical background of scattering phenomena. Similarly, temperature-dependent absorption properties were introduced as a numerical input for laser transmission welding (LTW) process simulations of short glass fiber filled and unfilled PP and PA6 in Ref. [15]. The behavior about the absorption characteristics of the unfilled semi-crystalline polymers under varying temperature was however not highlighted. In addition, in the most of those studies, the temperature dependence in the thermo-optical properties of semi-crystalline thermoplastics was analyzed at single wavelength, as laser assisted heating is performed at monochromatic wavelength. However, in case of IR heating of semi-crystalline polymers, the temperature dependence in their optical properties required to be characterized in a large spectral range. Because, the radiation emitted from an IR lamp is not at a monochromatic wavelength but in a spectral range, unlike to the laser heating.

In this paper, a novel experimental and numerical approach for radiation heat transfer in semi-crystalline thermoplastics is proposed. The experimental and numerical approaches were analyzed for the case of IR heating of PE polymer. For the study, the temperature-dependent transmittance and reflectance characteristics of semi-crystalline PE was experimentally analyzed considering different temperatures between 25 °C and 128 °C. Under heating condition, the variation in the optical scattering behavior inside of PE medium and its crystalline phase evolutions were analyzed considering two different transmittance measurements, namely directional-directional ($T_\lambda^{i,r}$ (T)) and directional-hemispherical transmittance ($T_\lambda^{i,\cap}$ (T)). The effect of both the measurements on the determination of the absorption characteristics of PE was highlighted. The analyses were extended characterizing the directional-hemispherical reflectance ($R_\lambda^{i,\cap}$ (T)) of PE. Assuming an optically homogeneous medium, the measured $T_\lambda^{i,\cap}$ (T) and $R_\lambda^{i,\cap}$ (T) were used to calculate an equivalent temperature-dependent extinction coefficient (β_λ (T)). The calculated β_λ (T) were then used as numerical input so that the temperature dependence of absorbed radiative energy by the PE medium was taken into account in the model. Thus, the effect of optical scattering on the absorption characteristics of PE under varying temperature was considered without modeling the spatial distribution of the scattered light intensity, which offers computationally cost-effective numerical solutions. The computational study was carried out using an in-house developed radiation heat transfer algorithm -RAYHEAT- and the commercial software -COMSOL Multiphysics®-, where iterative closed-loop computations were performed establishing a connection between them via MATLAB LiveLink. In order to assess the accuracy of the model, IR heating experiments were performed using PE plates and, surface temperature measurements were obtained via IR thermography and contact thermocouples. Since the spectroscopic analyses showed that PE has three narrow bands where the polymer is close to be opaque, an experimental methodology was developed for obtaining the most accurate surface temperature measurements on PE via IR thermography. The accuracy of IR thermography of PE was analyzed performing successive IR thermography tests.

2. Characterization of temperature-dependent optical properties

2.1. Materials and sample preparations

Highly crystalline linear PE was used in this study. The averaged peak crystalline melting temperature and the weight-average molecular weight ($\overline{M_w}$) of the studied PE resin is around 132 °C and 150000 Daltons, respectively. The PE polymer in the form of pellets was injection molded and square PE plates with dimensions of 78 × 78 × 2.2 mm were fabricated. In order to analyze the temperature-dependent optical characteristics of PE, the injected plates were then cut into small pieces and compressed in a heating chamber at 180 °C in order to obtain thin samples with controlled thickness. All the compressed samples were quenched into liquid nitrogen (LN_2) immediately after opening the heating chamber. The main reason for quenching the compressed PE samples is to achieve the closest crystalline structure possible in comparison to the crystalline structure of the industrial PE precursors used for actual thermoforming processes of PE. In the actual thermoforming process of PE in industry, the PE precursors are fabricated under rapid cooling conditions prior to the IR heating and forming steps, where their crystalline phase is greatly affected by cooling speed. The samples were prepared under the identical preparation conditions in three different thicknesses (0.25, 0.50 and 0.75 mm). The thickness measurements of the compressed samples showed that the thickness variation in each sample is around ± 20 μm. In addition, the surface roughness of the compressed PE samples was analyzed regarding the surface characteristics of the metal compression plates of the heating chamber. Due to the semi-transparency of PE polymer, its surface roughness could not be obtained appropriately using a non-contact profilometer. Instead, the tests were conducted using the compression plates, where its surface roughness was assumed

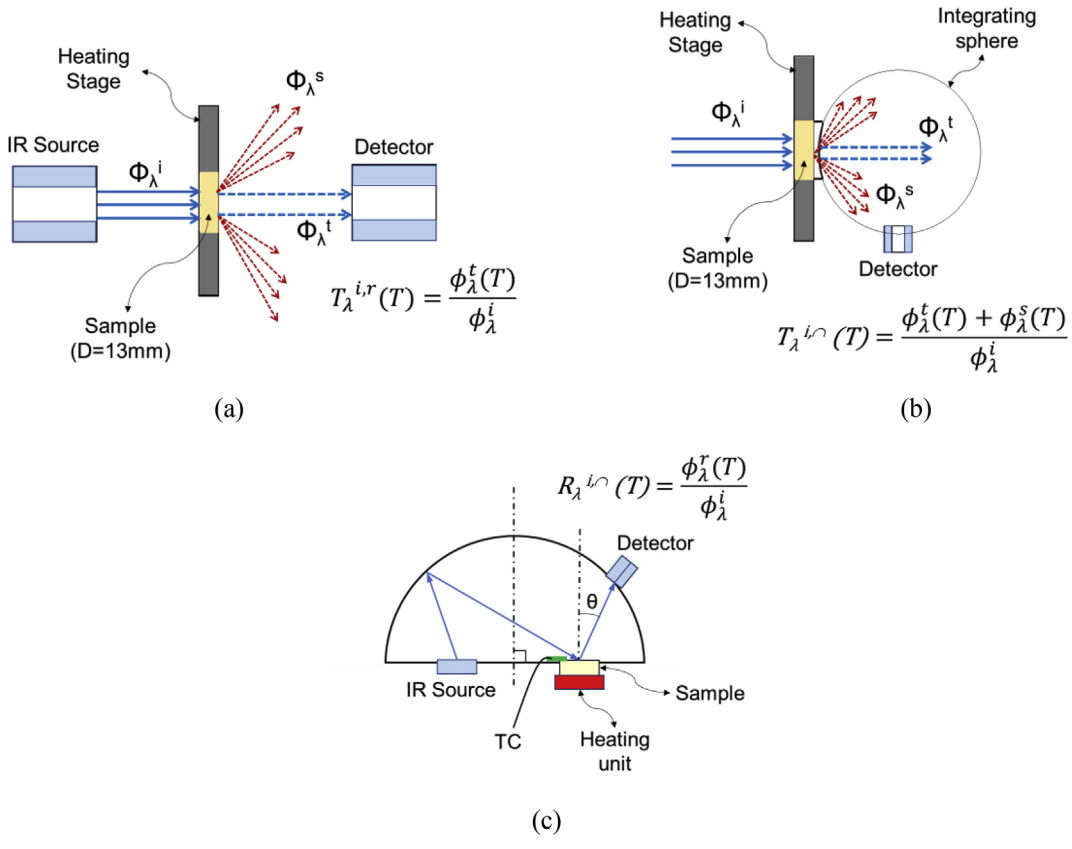

Fig. 1. The test setups for $T_\lambda^{i,r}$ (a), $T_\lambda^{i,\cap}$ (b) and $R_\lambda^{i,\cap}$ (c) measurements.

identical to the PE samples. The arithmetic mean (R_a) and root-mean-square roughness (R_q) of the compression plates were found around 0.37 and 0.46 μm, respectively. The further details related to the sample preparation can be found in Ref. [5].

Apart from the small samples used for the temperature-dependent optical properties measurements, several numbers of the fabricated PE plates were kept for the IR heating experiments to perform preliminary IR thermography analyses and the numerical-experimental comparisons that are presented in Section 4.

2.2. Test methodology for temperature-dependent spectroscopic measurements

The temperature dependency in the optical properties of PE was analyzed performing $T_\lambda^{i,r}$ (T), $T_\lambda^{i,\cap}$ (T) and $R_\lambda^{i,\cap}$ (T) tests. The overview of the test setups used for $T_\lambda^{i,r}$ (T), $T_\lambda^{i,\cap}$ (T) and $R_\lambda^{i,\cap}$ (T) measurements are schematically displayed in Fig. 1 (a), (b) and (c), respectively. The $T_\lambda^{i,r}$ (T) tests were done using a Fourier Transform Infrared (FT-IR) spectrometer (Bruker Vertex 70) and, the $T_\lambda^{i,\cap}$ (T) tests were performed employing another FT-IR spectrometer (PerkinElmer 950) combined with an integrating sphere. For both the $T_\lambda^{i,\cap}$ (T) and $T_\lambda^{i,r}$ (T) tests, a heating stage (Bruker A599) was used so that the PE samples, which has a diameter (D) of 13 mm, were mounted into the heating stage and, heated by conduction during the measurements. The heating stage was positioned at the entrance port of the integrating sphere for the $T_\lambda^{i,\cap}$ (T) tests whereas no integrating sphere was used in the $T_\lambda^{i,r}$ (T) tests. Considering an optically heterogeneous medium, the incident light flux (ϕ_λ^i) may be either directly transmitted or scattered. Hence, as shown in Fig. 1 (b), transmittance tests performed with integrating sphere enable to detect both the forward-scattered (ϕ_λ^s) and directly transmitted (ϕ_λ^t) light fluxes which travel through such a heterogeneous medium. The identical temperature steps were adopted for both types of the transmittance test. Between the two consecutive measurement steps of both the $T_\lambda^{i,\cap}$ (T) and $T_\lambda^{i,r}$ (T) tests, the samples were heated up in a monotonically increasing manner and waited for 2 min to reach a steady-state temperature.

The $R_\lambda^{i,\cap}$ (T) tests were done employing SOC-100 model Hemispherical Directional Reflectometer (HDR) built by Surface Optics Corporation. The average waiting time for the $R_\lambda^{i,\cap}$ (T) tests was around 5 min where the samples were also heated by conduction using the heating unit of the SOC-100 HDR (Fig. 1 (c)). Since two different heating units were used for heating the samples in the temperature-dependent transmittance and reflectance tests, the waiting time for reaching steady-state temperature at each consecutive temperature step was different. In addition, for the $R_\lambda^{i,\cap}$ (T) tests, a thin piece of black metal plate was mounted between the heating unit and the PE sample as our previous studies showed that PE is highly semi-transparent [5,16]. Thanks to this step, the amount of radiation flux that is transmitted through the sample medium would not reflect back and received by the detector, which may avoid having an erroneous reflectance measurement.

The $T_\lambda^{i,\cap}$ (T) and $R_\lambda^{i,\cap}$ (T) tests were done using the 0.25, 0.50 and 0.75 mm thick PE samples whereas the $T_\lambda^{i,r}$ (T) tests were carried out using 0.75 mm thick samples. It should be mentioned here that the crystalline morphology of PE may be altered under varying temperature, in particular the crystalline substructures, namely the lamellae [17,18]. Hence, several numbers of samples were prepared in identical condition and each sample was used for each individual $T_\lambda^{i,r}$ (T), $T_\lambda^{i,\cap}$ (T) and $R_\lambda^{i,\cap}$ (T) test. The reason behind this is to eliminate potential change in the optical characteristics of PE that may be induced by the difference in the crystalline phase of an already-tested sample. However, the waiting time at the each temperature step of all the $T_\lambda^{i,r}$ (T), $T_\lambda^{i,\cap}$ (T) and $R_\lambda^{i,\cap}$ (T) tests may allow melting-reorganization in the crystalline phase of linear PE [19], especially at the temperatures close to its melting range. Nevertheless, it was assumed that the potential effect of the reorganization in the crystalline phase of PE to the optical

Table 1
The PE samples and the testing characteristics of the $T_\lambda^{i,r}$ (T), $T_\lambda^{i,\cap}$ (T) and $R_\lambda^{i,\cap}$ (T) tests.

Type of measurement	Sample thickness (mm)	Temperature steps (T_{actual} (°C)) of the measurements	Spectral range of the measurements
$T_\lambda^{i,r}$ (T)	0.75	25, 48, 71, 84, 97, 110, 114, 116, 118, 120, 121, 122, 123, 126, 128	0.8–2.5 μm
$T_\lambda^{i,\cap}$ (T)	0.25, 0.50 and 0.75		0.25–2.5 μm
$R_\lambda^{i,\cap}$ (T)	0.25, 0.50 and 0.75	25, 71, 97, 103, 107,110, 114, 118, 120, 124, 128	2–25 μm

characteristics is negligible. In total, the transmittance and reflectance measurements were performed at 15 and 11 different temperature steps, respectively. The ambient temperature during the spectroscopic measurements was 25 °C. Overview of all the $T_\lambda^{i,r}$ (T), $T_\lambda^{i,\cap}$ (T) and $R_\lambda^{i,\cap}$ (T) tests are presented in Table 1. In the table, the temperature steps represent the actual temperature (T_{actual}) on the sample surface where the measurements were done. It was observed that the set temperature (T_{set}) on both the heating devices and, the T_{actual} on the measurement zone were different. Thus, preliminary tests were done for determining the T_{actual} of each adopted measurement step prior to the $T_\lambda^{i,r}$ (T), $T_\lambda^{i,\cap}$ (T) and $R_\lambda^{i,\cap}$ (T) tests.

It should be noted that the degree of crystallinity (X_c (%)) of all the PE samples was determined via calorimetric analyses, prior to the temperature-dependent spectroscopic measurements. It was found that X_c of all the quenched PE samples was around 67%, whereas, under heating, this value was reduced to around 62%, 57% and 34% at 100 °C, 115 °C and 128 °C, respectively. Apart from determining the T_{actual} for all the tests, the temperature variations alongside the polymer surface was investigated for the heating case applied in both the $T_\lambda^{i,r}$ (T) and $T_\lambda^{i,\cap}$ (T) tests. The heating stage used in these tests heats the material from its edge, and therefore the middle of the sample -where transmittance measurements are performed-has a lower temperature which may be critical in terms of accuracy in the measurements. The preliminary tests dedicated for analyzing these points were carried out using poly (ethylene terephthalate) (PET) samples. For each temperature step, the temperature profile on the PET surface was recorded using an IR camera (FLIR SC325). PET was chosen as a reference material for these analyses as, it is opaque in the operating range of a typical IR camera in contrast to PE polymer [20]. Hence, a reliable surface temperature on PET could be obtained via IR thermographic measurements [21]. It was then assumed that the temperature recorded from PET surface is identical to the PE samples considering that conduction and convection heat transfer are identical for both the polymers. Obtaining the temperature profile from the edge through the middle of the sample enables to adjust the size of the incident light that is transmitted through the sample, which represents transmittance measurement zone. Because the temperature variations are desired to be negligibly small in the transmittance measurement zone so that a reliable correlation between the actual measured temperature and the transmittance can be obtained at each measurement step. Thus, the beam width of the incident light that is sourced from the spectrometer was set to 1.5 mm since the temperature variation inside of this zone was lower than 0.3 °C. For the $R_\lambda^{i,\cap}$ (T) tests, the preliminary tests were done using 0.5 mm thick PE samples and the T_{actual} of each measurement step was determined using the thermocouple (TC) of the heating unit in SOC-100 HDR. As shown in Fig. 1 (c), the TC is attached on the top surface of the sample where also the reflectance measurements are performed. Since the sample is heated from below in these tests, the temperature variation through its thickness is likely to happen. However, it may be relatively small considering the thicknesses of the tested samples, which are between 0.25 and 0.75 mm. Hence, it was assumed that the effect of thickness on the top surface temperature of all the tested samples is negligibly small. Therefore, T_{actual} of each measurement step obtained using 0.5 mm thick samples was also adopted for 0.25 mm and 0.75 mm thick samples. In addition, thermal coupling agent was used between the heating unit and the sample to secure good thermal contact in each $R_\lambda^{i,\cap}$ (T) test.

2.3. Temperature-dependent thermo-optical properties of PE

As aforementioned, the crystalline structure of semi-crystalline polymers introduces an optically heterogeneous medium which induces optical scattering and complex radiation transport inside of polymer medium. Potential evolution in their crystalline structure under varying temperature may therefore causes to change the optical scattering behavior. The question arises here about the accuracy of the temperature-dependent absorption characteristics of PE medium, parametrized as β_λ (T) in this study. β_λ of a semi-transparent medium is theoretically calculated using the medium's reflectance and transmittance characteristics [22,23]. Hence, it is of prime importance to understand which type of optical measurement may provide the most accurate calculation on the temperature-dependent absorption behavior in the optically heterogeneous and semi-transparent PE medium. In order to investigate this point; a critical analysis was carried out considering the temperature-dependent $T_\lambda^{i,r}$ (T) and $T_\lambda^{i,\cap}$ measurements on the 0.75 mm thick identically prepared PE samples. In Fig. 2, the $T_\lambda^{i,r}$ (T) of a PE sample was compared to its $T_\lambda^{i,\cap}$ values that were measured at 25 °C. In the figure, the $T_\lambda^{i,r}$ (T) measurements are labeled regarding the temperature at which they were obtained. As displayed in the figure, there is a significant difference between the measured $T_\lambda^{i,r}$ and $T_\lambda^{i,\cap}$ of the identical PE sample. The dashed line displayed in the figure show that the $T_\lambda^{i,\cap}$ of the sample is around 72% at 1 μm, whereas its $T_\lambda^{i,r}$ measured at 25 °C is around 4%. It is a clear evidence that significant part of the transmitted light flux is actually forward-scattered as the $T_\lambda^{i,r}$ measurements lack in detecting all the transmitted light flux through the optically heterogeneous medium. It should also be noted that some amount of the light flux may also be back-scattered inside of the polymer medium and may not enter the integrating sphere [24]. This point is discussed further in Ref. [5] based on the comparison between the $T_\lambda^{i,r}$ and $T_\lambda^{i,\cap}$ of PE samples prepared in different thicknesses and analyzed at room temperature. It was observed that the amount of back-scattered light flux may be negligible in comparison to ϕ_λ^s considering the same spectral range, presented in Fig. 2.

At higher temperatures, the $T_\lambda^{i,r}$ (T) values increases and surpasses the $T_\lambda^{i,\cap}$ that was obtained at 25 °C, which can be attributed to the weaker optical scattering under heating condition. Once the

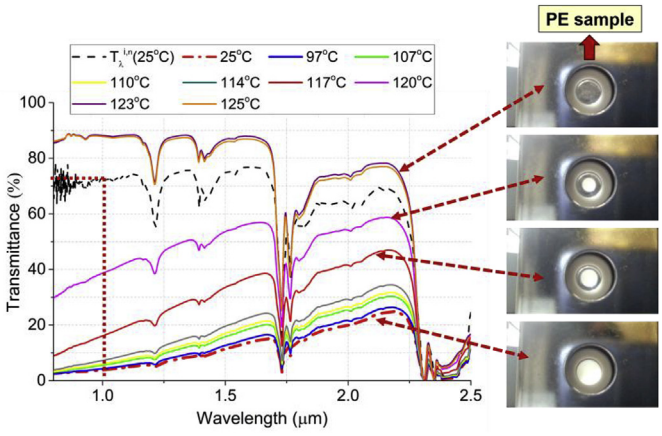

Fig. 2. Comparison between the $T_\lambda^{i,r}$ (25 °C) and $T_\lambda^{i,\cap}$ (25 °C) of the 0.75 mm thick PE sample and, the evolution of its $T_\lambda^{i,r}$ (T) under varying temperature.

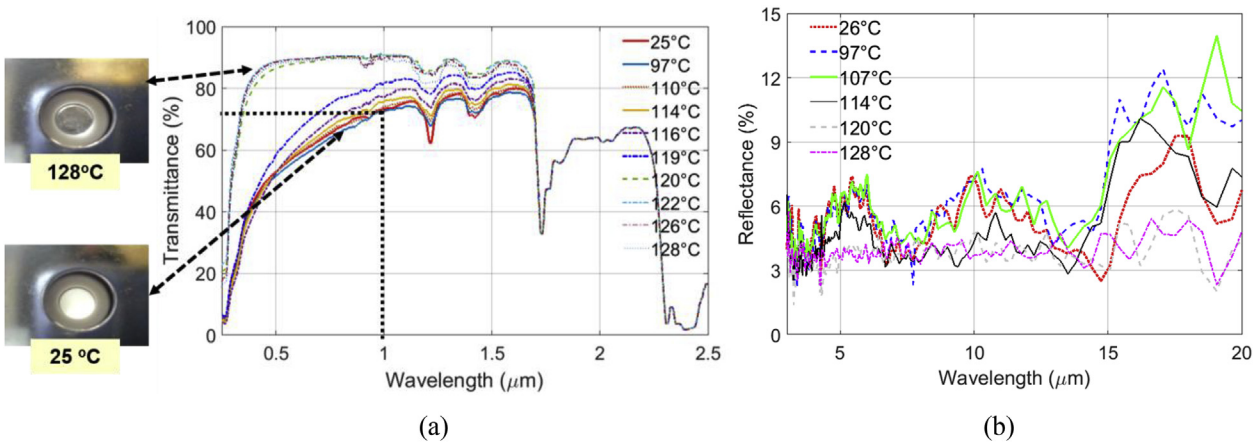

Fig. 3. Typical trend obtained in the $T_\lambda^{i,\cap}$ (a) and $R_\lambda^{i,\cap}$ (b) measurements of PE polymer under varying temperature.

temperature is above 114 °C a dramatic increase in the $T_\lambda^{i,r}$ (T) is seen. It reaches its maximum values above 120 °C which is around 90% transmittance at 1 μm. The changes in the color of the polymer under heating can also be seen clearly in the successively taken photos during the test (Fig. 2). The PE polymer has a milky color at lower temperatures and becomes totally transparent after 120 °C. The reason behind these changes is obviously related to crystalline structure evolutions since the optical scattering becomes weaker at higher temperatures, especially closer to the melting range of PE [5]. In addition, the comparisons between the $T_\lambda^{i,r}$ (T) and $T_\lambda^{i,\cap}$ of an identical PE sample indicates that the amount of scattered and transmitted light may not be negligible for optically heterogeneous semi-crystalline PE medium, otherwise its temperature-dependent absorption characteristics may be overestimated, due to underestimation of transmittance levels. Consequently, in this study, the temperature-dependent absorption characteristics in semi-crystalline PE was determined characterizing its $T_\lambda^{i,\cap}$ (T) and $R_\lambda^{i,\cap}$ (T).

In Fig. 3 (a) and (b), the typical trend obtained in each $T_\lambda^{i,\cap}$ (T) and $R_\lambda^{i,\cap}$ (T) tests are presented, respectively. It is seen in Fig. 3 (a) that the $T_\lambda^{i,\cap}$ of the 0.75 mm thick sample in the range 0.4–1.7 μm increases under heating where the increase is more pronounced after 116 °C. This corresponds to temperatures close to the melting range of PE [5]. In addition, no significant change was observed in $T_\lambda^{i,\cap}$ of all the tested PE samples for the wavelengths greater than 1.7 μm. It was thus assumed that $T_\lambda^{i,\cap}$ remains unchanged under heating considering the spectrum between 1.7 and 2.5 μm. Furthermore, similar to the trend seen in the $T_\lambda^{i,r}$ (T) measurements, the $T_\lambda^{i,\cap}$ at 1 μm of the 0.75 mm thick sample that is around 72% at 25 °C increases up to 90% at 128 °C. Hence, one can analyze that the $T_\lambda^{i,r}$ (T) and $T_\lambda^{i,\cap}$ of the identically prepared different PE samples show the same level of transmittance once the polymer becomes transparent above 120 °C. It is a clear evidence that PE medium becomes completely optically homogeneous above these temperature, since the $T_\lambda^{i,r}$ (T) and $T_\lambda^{i,\cap}$ measurements obtained from two different FT-IR spectrometer are very close. The variation between all the identically prepared and tested samples was found around 0.3–0.5% which can be attributed to small variations in the sample thicknesses.

In addition, the temperature dependent trend in the $T_\lambda^{i,\cap}$ values of 0.25 and 0.5 mm thick PE samples showed similar behavior to the one presented in Fig. 3 although, small variations were observed about the temperature at which their $T_\lambda^{i,\cap}$ greatly increases. This might be due to the difference in their optical scattering characteristics that may result from some differences in their crystalline morphology. Indeed, although all the PE samples were quenched into LN_2, the difference in sample thicknesses may cause some variations in their cooling history and thus in morphology of the linear PE [25].

In contrast to the trend in $T_\lambda^{i,\cap}$ (T), an inverse relation between the $R_\lambda^{i,\cap}$ of PE and temperature was observed. As shown in Fig. 3 (b), the temperature change is less effective on the reflectance of PE in comparison to its temperature-dependent transmittance. Similar to the findings in the $T_\lambda^{i,\cap}$ (T) tests, consistency was observed in the decreasing trend in the $R_\lambda^{i,\cap}$ (T) of all the tested PE samples tests above 107 °C. For the sake of brevity in Fig. 3 (a) and (b), the temperature dependent trend in the $T_\lambda^{i,\cap}$ and $R_\lambda^{i,\cap}$ values are presented considering only certain number of measurement steps.

In previous studies [5,26], it was found that the strong coupling between crystalline morphology and the transmittance characteristics of PE becomes negligible in MIR range (2–25 μm). It was therefore assumed in this study that the transmittance characteristics of PE in MIR range are independent of temperature. Hence, $T_\lambda^{i,\cap}$ of the PE samples measured at room temperature was adopted for this range. Conversely, no temperature-dependent $R_\lambda^{i,\cap}$ (T) measurements were able to be obtained for the wavelengths lower than 2 μm, due to the limitations in the spectral response of the employed FT-IR devices. Therefore, temperature dependency in the reflectance characteristics of PE was assumed negligible for the wavelengths lower than 2 μm. Although this is not a rigorous assumption, in the corresponding spectral range, the further $R_\lambda^{i,\cap}$ tests were done at 25 °C using PE samples prepared with identical thicknesses, but with different crystalline structures where the samples were annealed under stepwise cooling. It was observed that the crystalline structure of PE has a slight effect on its $R_\lambda^{i,\cap}$ values. It was thus assumed that a change in the crystalline structure under varying temperature has a negligible effect on the $R_\lambda^{i,\cap}$ of PE.

Based on the measured $T_\lambda^{i,\cap}$ (T), $R_\lambda^{i,\cap}$ (T) and the conservation of radiative energy (Equation (1)), the fraction of absorbed energy, also called absorbance ($A_\lambda^{i,\cap}$ (T)) can be determined for each temperature step. Assuming an optically homogeneous semi-transparent medium, β_λ of PE polymer can be calculated at each corresponding temperature step regarding the transmittance and the reflectance characteristics of its medium (Equation (2)) [22].

$$A_\lambda^{i,\cap}(T) + T_\lambda^{i,\cap}(T) + R_\lambda^{i,\cap}(T) = 1 \tag{1}$$

$$R_\lambda^{i,\cap}(T) = \rho_\lambda\left[1 + \tau_\lambda^2\frac{(1-\rho_\lambda)^2\tau_\lambda^2}{1-(\rho_\lambda\tau_\lambda)^2}\right] \quad \text{and,} \quad T_\lambda^{i,\cap}(T) = \frac{(1-\rho_\lambda)^2\tau_\lambda}{1-(\rho_\lambda\tau_\lambda)^2} \text{where;}\ \tau_\lambda = e^{-\beta_\lambda . x} \tag{2}$$

In Equation (2), x, τ_λ and ρ_λ represent thickness, intrinsic transmittivity and reflectivity of the PE, respectively [22]. The computation of β_λ at each temperature step was carried out in MATLAB adopting an inverse method based on SQP (Sequential Quadratic Programming) estimation algorithm. In the method, double objective function (J) was created considering the experimental and numerically computed reflectance ($R_{numerical}$ (T)) and transmittance ($T_{numerical}$ (T)) values

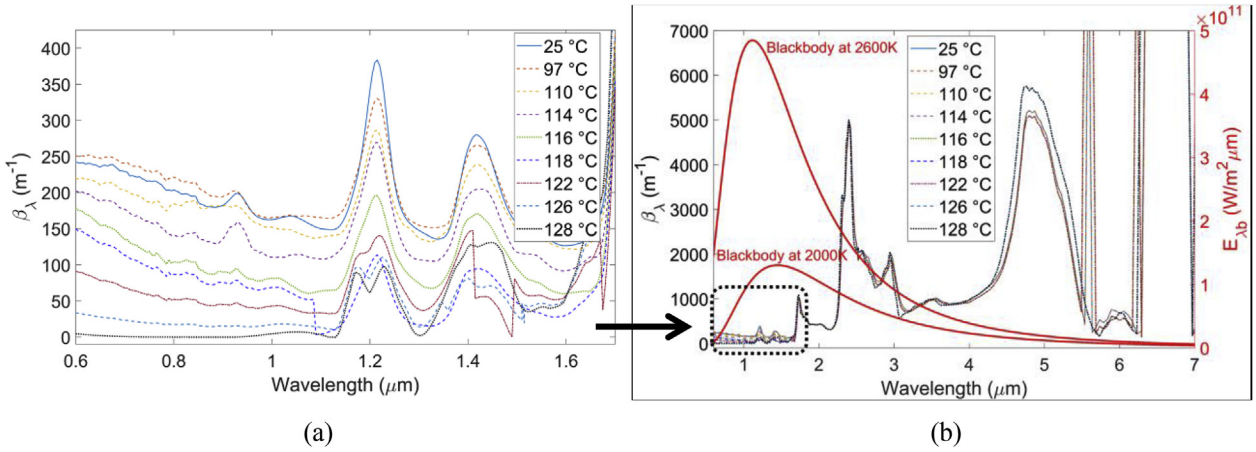

Fig. 4. The significant variation in β_λ (T) of PE polymer between room temperature and 128 °C (a) and the β_λ (T) values in the spectral ranges of a black body at 2000 and 2600 K (b).

(Equation (3)). $T_{numerical}$ and $R_{numerical}$ was computed adopting Equation (2) and initial guessed values for ρ_λ and τ_λ. The iterative-based computation was performed until the solver error condition is satisfied at which the value of J is smaller than the tolerance value (1e-6). At the end the iterative computation, the ρ_λ, τ_λ values, and eventually β_λ was determined. This computation was done for the each measured $T_\lambda^{i,\cap}$ (T) and $R_\lambda^{i,\cap}$ (T) values at each corresponding temperature step. The in-house developed estimation algorithm is explained further in Ref. [27].

$$J = \left| \frac{T_\lambda^{i,\cap}(T) - T_{numerical}(T)}{T_\lambda^{i,\cap}(T)} \right| + \left| \frac{R_\lambda^{i,\cap}(T) - R_{numerical}(T)}{R_\lambda^{i,\cap}(T)} \right| \quad (3)$$

In Fig. 4 (a) and (b), the computed β_λ (T) values are presented considering the spectrum between 0.6 and 7 μm. Again, for the sake of clarity, some of the computed β_λ (T) values are not presented in the figure. The temperature dependence in β_λ is illustrated in Fig. 4 (a), including the spectrum between 0.6 and 1.6 μm. It is clearly seen that the trend in β_λ (T) is monotonically decreasing under heating. This may be plausible, as the increase in the $T_\lambda^{i,\cap}$ (T) values is significant in this spectrum, as presented in Fig. 3 (a). In terms of IR heating with an IR lamp, such an evolution in the thermo-optical properties of semi-crystalline polymers may be crucial as considerable amount of radiation energy may be emitted in the corresponding spectrum. To illustrate this point, the spectral ranges of the black body emissive power ($E_{\lambda b}$ (W/m^{2}μm)) at 2000 and 2600 K were displayed together with the β_λ (T) of PE in Fig. 4 (b). Considering the fact that a halogen IR lamp used for injection stretch blow molding (ISBM) processes has a temperature around 2000–2600 K, maximum emission wavelength (λ_{max} (μm)) of the lamp should be theoretically around 1.1–1.4 μm, regarding to Wien's displacement law [22,23]. In addition, nearly 95% of total energy emitted by such an IR lamp lies between $\lambda_{max}/2$ and $5\lambda_{max}$ which reflects a spectral range roughly between 0.6 and 7 μm [20,22,23]. It may therefore be concluded that the temperature dependence in the thermo-optical properties of semi-crystalline PE seen in NIR range may have a significant effect on the amount of absorbed energy, due to both high level of emitted radiation by IR lamp and the variation in its absorption characteristics.

Based on the temperature-dependent behavior observed in the $T_\lambda^{i,\cap}$ (T) tests, the $T_\lambda^{i,\cap}$ (T) measurements obtained between 25 °C and 97 °C were ignored as the change in temperature did not cause any variation in the measured values. By the same token, $R_\lambda^{i,\cap}$ (T) measurements between 25 °C and 107 °C were ignored. The main reason to neglect the measurements that shows no temperature dependency is to reduce computational cost. By reducing the number of numerical input, it will eventually reduce the number of iteration steps of the closed-loop computations, which is explained in detail in Section 3.2. At the end, the β_λ (T) was computed at 12 different temperature steps between 25 °C and 128 °C. Each calculated β_λ (T) was used as input in the numerical model for computing the radiative power absorbed by the polymer medium, namely radiative source term ($\nabla.q_r$ (W/m^3)), for each corresponding temperature step. Prior to the $\nabla.q_r$ computations, the β_λ (T) was integrated for the spectral range of 95% of the emitted energy from an IR lamp that is between $\lambda_{max}/2$ and $5\lambda_{max}$ (Equation (4)). This spectral range can be determined by knowing the temperature of IR emitter and adopting Wien's displacement law. It should also be noted that I_λ° in the equation below represents the incident radiation intensity emitted from an IR lamp.

$$\overline{\beta}(T) = \frac{\int_{\lambda_1=\lambda_{max}/2}^{\lambda_2=5\lambda_{max}} \beta_\lambda(T) I_\lambda^o d\lambda}{\int_{\lambda_1=\lambda_{max}/2}^{\lambda_2=5\lambda_{max}} I_\lambda^o d\lambda} \quad (4)$$

3. Background of the numerical model

3.1. Temperature-dependent thermophysical properties

The temperature dependence in the thermophysical properties of PE, namely thermal conductivity (k (W/mK)) and specific heat capacity (C_p (J/kgK)), were taken into account in the model. It is known that temperature-dependence in k of semi-crystalline polymers is strongly affected by their crystalline structure [1,17]. The temperature-dependent k of PE used in the model was adopted from literature [1]. The temperature-dependent variation of the adopted k values was presented in our previous study [5]. Although, variations in X_c may result in an increase of the conductivity of semi-crystalline polymers [1,19,28], it was assumed here that k was independent of X_c. In addition, highly ordered crystalline structures that form in certain directions may introduce anisotropy in the thermal conductivity of semi-crystalline polymers as stressed in Refs. [28,29]. Such a potential effect was neglected in the numerical model and isotropic conductivity was assumed for PE.

The apparent heat capacity ($C_{p,}^{apparent}$ (J/kgK)) of the PE, that represents the total energy required for increasing the temperature of unit mass of polymer, was measured employing a power compensated differential scanning calorimeter (DSC). As shown in Fig. 5, the $C_{p,}^{apparent}$ of PE under heating conditions is not strictly monotonic but exhibits a phase transition related to the melting of the crystalline phase of PE. The temperature-dependent apparent heat capacity ($C_{p,}^{apparent}$ (T)) can thus be described with Equation (5) considering the temperature-dependent specific heat capacity (C_p (T)) and the phase transition

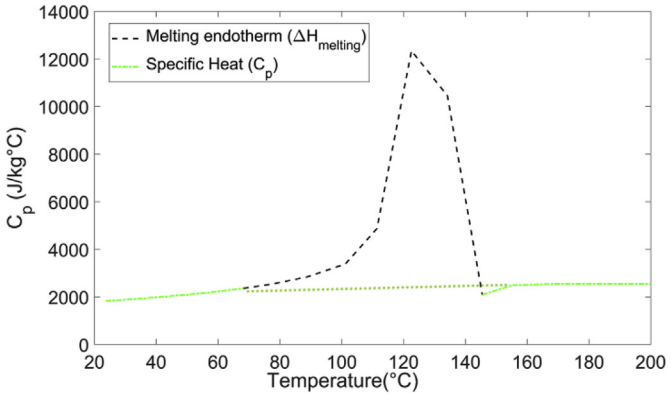

Fig. 5. Superposition of C_p (T) and $\Delta H_{melting}$ of PE obtained from the DSC measurements.

enthalpy $\Delta H_{melting}$ (J/g) [17,30]. For the sake of simplicity, the melting kinetic was however not modeled and the $C_{p,}^{apparent}$ (T) was directly used as an input in the numerical model.

$$C_p^{apparent}(T) = C_p(T) + \frac{\Delta H_{melting}}{dT} \tag{5}$$

Under heating condition, the potential reduction in X_c due to partial melting of crystalline phase may also cause to change the density (ρ) of PE [17,19,31]. As a consequence, the specific volume ($\bar{V}$) of the material -which is reciprocal of ρ-may change significantly under varying temperature [1,32] which physically addresses the thermal expansion of polymer medium. Considering isochoric simulations, such expansion in polymer geometry was not taken into account hence; the spatial expansion in the node coordinates of the modeled mesh elements is ignored under varying temperature. On the contrary, in terms of computational cost for radiation transport and the absorbed radiation energy in the model, the consideration of this effect would introduce complexity as the ray tracing computations should be rerun at each computational step. Therefore, temperature-dependent ρ of PE was considered as negligible in the model. Nevertheless, the initial value of the ρ was defined as a function of the X_c of PE samples in the model. The two-phase model was adopted for defining the global density (ρ_{global}) of PE regarding the fraction of crystalline and amorphous phases (Equation (6)) [31,33]. The ρ_{global} in Equation (6) represents the macroscopic density of simulated polymer geometry.

$$\rho_{global} = \frac{1}{\left(\frac{X_{crystalline}}{\rho_{crystalline}}\right) + \left(\frac{1 - X_{crystalline}}{\rho_{amorphous}}\right)} \tag{6}$$

In this study, X_c of PE was taken as 67% which corresponds to the average value measured on the injected PE plates and obtained from the calorimetric analyses. The density of crystalline and amorphous phases of PE that are appeared in Equation (6) were adopted from literature [19,34], as 1000 and 855 kg/m^3, respectively. Hence, ρ_{global} was defined as 952 kg/m^3 in the model.

3.2. Radiation heat transfer modeling approach based on temperature-dependent thermo-optical properties of semi-crystalline thermoplastics

As aforementioned, absorbed radiation inside of PE polymer medium was computed using an in-house developed radiation heat transfer algorithm -RAYHEAT-. In the algorithm, thermal radiation computations are done based on Ray Tracing method so that the emitted radiation from an IR lamp is modeled as traveling in straight lines, called rays. In RAYHEAT, only the tungsten filament of an IR lamp is taken into account. Therefore, the length of each IR lamp is modeled considering the length of its tungsten filament. Each single filament is modeled by equivalent cylinders where its spiral form is neglected. In this study, the diameter of a cylindrical filament is modeled as 2.15 mm, in accordance with the IR heating experiments presented in Section 4. The emitted energy from the filament of a halogen IR lamp is assumed Lambertian and the source is considered as a grey body. In addition, the discretization of the ray from the surface of modeled filament was performed adopting a stochastic approach [35,36]. Thanks to this, a numerous number of rays are released randomly from the cylindrical surface of filament. The total amount of the emitted energy is uniformly shared among all the rays. The further explanations about the released rays from the modeled filament and the schematical illustration of the released rays in RAYHEAT can be found in Ref. [35]. In the model, the emitted rays which do not touch the polymer geometry is considered lost. Once a ray intersects the polymer geometry, some of the carried energy is reflected and the remaining part of the energy is transmitted through the polymer medium, where the direction of each ray is changed at the air/polymer interface due to refraction. The change in the direction of each ray is computed based on Snell-Descartes law in RAYHEAT, as explained in Ref. [35]. The refractive indices of air and PE medium were adopted in this study as 1 and 1.54 [7], respectively. The current version of RAYHEAT is based on optically homogeneous medium assumption. Therefore, the absorption of radiative energy inside of PE medium is computed following the Beer-Lambert Law, according to Equation (7) [22].

$$\frac{dI_\lambda}{dz} = -\beta_\lambda(z) I_\lambda(z) = -(\kappa_\lambda(z) + D_\lambda(z)) I_\lambda(z) \tag{7}$$

The radiative power absorbed by the polymer medium, $\nabla.q_r$, at the depth "z" is defined with Equation (8), at which β_λ is the sum of both absorption (κ_λ) and scattering coefficients (D_λ):

$$\nabla \cdot q_r(z) = \int_0^\infty -\beta_\lambda I_\lambda(0) e^{-\beta_\lambda z} d\lambda = \int_0^\infty -(\kappa_\lambda + D_\lambda) I_\lambda(0) e^{-(\kappa_\lambda + D_\lambda) z} d\lambda \tag{8}$$

The working algorithm of the model is displayed schematically in Fig. 6. As RAYHEAT is a MATLAB-based code, the iterative closed-loop between RAYHEAT and COMSOL Multiphysics® was established using MATLAB LiveLink feature which allows to transfer the computed $\nabla.q_r$ into COMSOL Multiphysics® as a numerical input at each time step. More specifically, in RAYHEAT, $\nabla.q_r$ was computed for each volumetric mesh element of the modeled polymer. Based on ray tracing approach, knowing to the information on the direction and the position of each ray entering the mesh element, the traveled distance inside of the element, and thus the attenuated power of each ray was computed. The accumulation of the attenuated power of all the rays traveling through each volumetric mesh element resulted to obtain the ∇.qr (W/m^3). The absorbed power of each mesh element was transferred from RAYHEAT to COMSOL using the MATLAB Livelink, where also the identical mesh elements were transferred.

The algorithm closed-loop then consisted in solving the transient heat transfer equation (Equation (9)) to predict the temperature field and in calling back RAYHEAT for updating the $\nabla.q_r$ of polymer medium regarding the computed temperature at the end of the corresponding iteration step. Therefore, the change in the amount of radiative energy absorbed by the PE medium during the time step - which is a function of the temperature and the spatial coordinates of the modeled mesh element-, is introduced in the model. As the calculated $\overline{\beta}(T)$ corresponds to the specific temperature step adopted for the temperature-dependent optical properties measurements, the numerical model interpolates $\nabla.q_r$, regarding the $\nabla.q_r$ of the two most close temperature steps in case that a computed temperature of a mesh element is somewhere between the adopted temperature steps. Otherwise, in a case that the temperature of a mesh element is lower than 25 °C or higher 128 °C, the model assigns the $\nabla.q_r$ computed at 25 °C or 128 °C, respectively. Such a temperature dependency at mesh scale was not considered for the thermophysical properties of PE thus, temperature-dependent k and C_p was assigned as a global parameter on the modeled PE medium. Hence

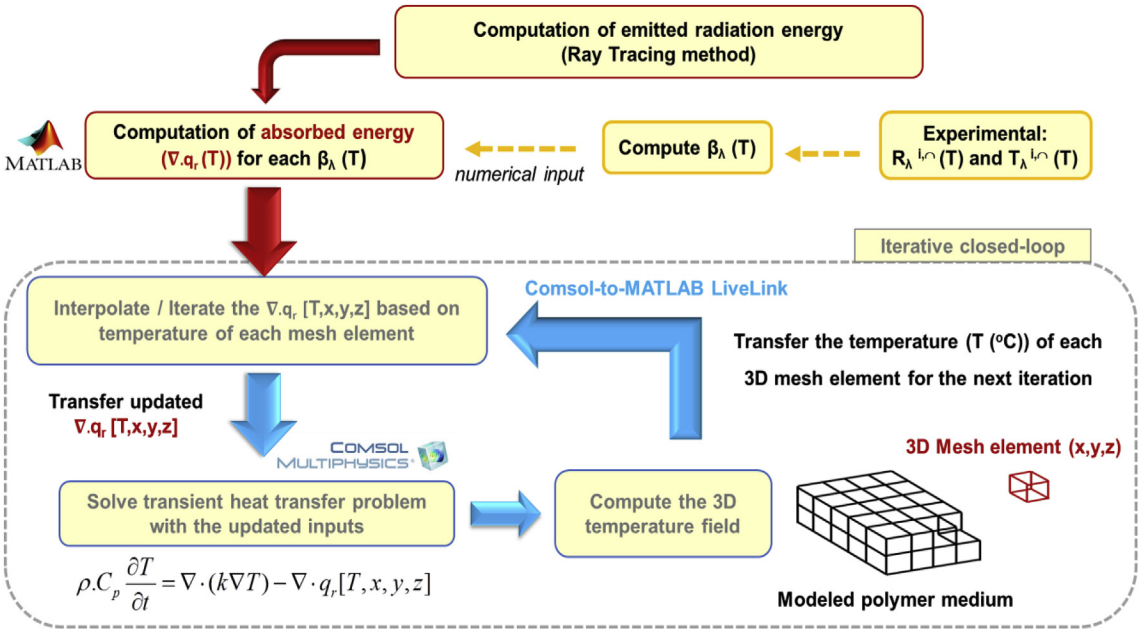

Fig. 6. Working algorithm of the developed numerical model.

the model computes the average temperature of the medium and updates these parameters at each computational time step.

$$\rho.\ C_p \frac{\partial T}{\partial t} = \nabla\cdot(k\nabla T) - \nabla\cdot q_r[T, x, y, z] \tag{9}$$

For thermal radiation computations based on ray tracing method, one of the important parameters is the number of modeled rays. In RAYHEAT, the effect of the number of ray on computational time and accuracy in the $\nabla.q_r$ was analyzed in Ref. [35] considering a square PET polymer plate heated by a single IR lamp. Their convergence studies suggested that the modeled rays greater than 1 million allows computing the absorbed radiation with an error less than 5% in RAYHEAT. Nevertheless, this suggestion may only be a reference for heating a simple geometry since an increase in the complexity of the geometry may also affect the accuracy of ray tracing computations. The accuracy may not be related to the ray tracing method as it is independent of geometric complexity but to the finite element meshing of the complex geometries and, its interaction to the intersected modeled rays [36].

In order to reduce the computation cost, the radiative energy that may be absorbed by each modeled 3D mesh element was computed and saved before starting the iterative closed-loop computations. Therefore, all the potential scenarios of the $\nabla.q_r$ values absorbed by each mesh element were computed regarding to all the integrated $\overline{\beta}\,(T)$ values. As aforementioned, the temperature steps where no variation in both $T_\lambda^{i,\cap}$ (T) and $R_\lambda^{i,\cap}$ (T) measurements seen was ignored for the $\overline{\beta}\,(T)$ calculations. Thanks to this, the number of potential scenarios for the computed $\nabla.q_r$ was reduced. In total, 12 different scenarios of $\nabla.q_r$ were created for 12 temperature steps. The boundary conditions and adopted parameters for both the cases of numerical simulations are presented in Table 2.

4. IR heating of PE and model predictions

4.1. IR heating experiments and thermal measurements

The accuracy of the numerical model was analyzed performing numerical-experimental comparisons for the case of IR heating experiments with the injection molded PE plates. The surface temperatures of the plates were measured via IR thermography and conventional contact thermocouples. Due to the semi-transparent medium of PE, preliminary experiments were done and, an experimental methodology was developed to obtain an accurate surface temperature via IR thermography. Subsequent preliminary IR thermography tests were performed using PET and PE plates where both the plates were geometrically identical. For all the IR heating experiments, a single IR lamp with a power of 1 kW (Toshiba JHS 235 V) was used. The cylindrical tungsten filament of the used IR lamp is 300 mm long, with a diameter of 2.15 mm.

4.1.1. IR thermography in semi-transparent PE medium and preliminary experiments

Regarding the transmittance behavior of PE, it has several narrow bands in MIR range where it shows very low transmittance and therefore it is close to be opaque [5,37,38]. Therefore, accurate IR thermographic measurements may be performed on PE surface only considering these spectral bands. A typical long-wave (LW) IR camera has

Table 2
The assumptions and input parameters adopted for the IR heating modeling of PE.

	Input parameter	Source of the parameter
Thermophysical properties of PE	k (W/mK)	Adopted from Ref. [1]
	$C_p^{apparent}$ (J/kgK)	DSC measurement (Fig. 5)
	ρ_{global} (kg/m^3)	Equation (6) and DSC measurements
Thermo-optical properties and the temperature-dependent absorption characteristics of PE	$\overline{\beta}\,(T)$	Calculated from the measured $T_\lambda^{i,\cap}$ (T) and $R_\lambda^{i,\cap}$ (T) at 12 temperature steps: 25, 97, 110, 114, 116, 118, 120, 121, 122, 123, 126, 128 °C
	$\nabla.q_r$ (T)	**For T < 25C:** $\nabla.q_r$ (25 °C) for all mesh elements **For 25 < T < 128 °C:** $\nabla.q_r$ (T) interpolated between the two closest temperature steps **For T > 128 °C:** $\nabla.q_r$ (128 °C) for all mesh elements

an operating spectral range between 7 and 14 μm [20] that cover two of the narrow spectral bands - around 7.6 and 13.6 μm, respectively-, at which PE has very low transmittance. However, as they are relatively narrow in comparison to the operating range of a typical IR camera, narrow bandpass (NBP) optical filters are necessary for quantitative IR thermographic measurements at these spectrums. At very first step, two different NBP optical filters (Northumbria Optical Coatings) close to 7.6 and 13.6 μm with bandwidths of ± 0.10 μm and ± 0.21 μm respectively were employed for the IR thermography of PE polymer. Both the filters were externally mounted and tested on two different IR cameras, namely a cooled LW IR camera (AGEMA 880) and an uncooled microbolometric IR camera (FLIR SC325). Thanks to this step, the sensitivity of both the employed IR cameras was analyzed at these preferably selected wavelengths. Initial analyses showed that the sensitivity of SC325 was too low for both the narrow bands, whereas enough sensitivity was recorded by the cooled LW IR camera only for the optical filter which has a spectrum between 7.5 and 7.7 μm [16,39]. It should be mentioned here that the operating spectral range of the employed LW IR camera is between 8 and 12 μm [21] indicating that spectral sensitivity of the IR detector is nominal in the corresponding range, whereas the detector is still sensitive at the wavelengths beyond, but close to, this range. Similarly, our sensitivity analyses showed that the LW IR camera is still sensitive enough in the spectral band around 7.6 μm. Nevertheless, an extra step was required to be applied to adjust the sensitivity of the IR camera in terms of obtaining a correct temperature related to the energy captured by the IR detector of the camera. Therefore, the optical filter mounted IR camera was calibrated using a black body calibration source (Landcal P550P) so that correlation between the IR radiation captured by the camera and a measured temperature was established. The calibration was done choosing reference temperatures on the black body source between 60 and 120 °C. The isothermal unit (UI) detected by the IR camera was registered for each corresponding reference temperature. Thus, a calibration curve was developed which enables to convert the detected energy emitted from the surface of the polymer to a temperature value. This calibration step is explained further in Ref. [39].

The question arises here about the sensitivity of the optical filter mounted IR camera in case of receiving the emitted energy from a real body, unlike a black body. This point was analyzed performing IR thermography tests using PET polymer. As aforementioned, PET behaves opaque in the operating spectral range of a typical IR camera. More specifically, it was reported in Ref. [21] that the optical penetration depth (D_p) of PET is around 30 μm in the spectral range between 5 and 20 μm. Hence, PET was used as a reference material for obtaining a reliable surface temperature via IR thermography and analyze the accuracy of the filter mounted LW IR camera. For the tests, a PET plate was heated using a single IR lamp and its back surface was monitored by the filter mounted LW IR camera (AGEMA880). The back surface temperature was also measured employing the other IR camera, FLIR SC 325. As no filer was mounted in this camera, and it operates between 7.5 and 13.5 μm [20], its measurements were considered as a reference for analyzing the accuracy of the optical filter mounted IR camera. In addition, one TC attached in the middle zone of the back surface for the comparisons. During the experiments, power of the IR lamp (P_{lamp} (%)) was changed between 15% and 35% of its nominal power and the temperature measurements were done once back surface temperature reached steady state. At the end, 5 different measurements were obtained between 50 and 70 °C. The surface temperature was read by the two IR cameras on the arbitrarily chosen zone which was next to the attached TC. All the recordings obtained by the IR cameras and the TC were compared at each steady-state temperature step (Fig. 7(a)). It was found that the maximum temperature difference (ΔT (°C)) between the values recorded by the two IR camera was around 1 °C (Fig. 7 (b)) verifying that the filtered energy captured by the optical filter mounted IR camera is sufficient to obtain accurate temperatures on a real body.

Apart from the sensitivity of the IR camera, the accuracy of the surface temperature measurements on PE was analyzed in terms of the D_p of PE in the spectral range where IR thermography was achieved. In our previous study [39], the D_p of PE was calculated considering the spectral band of the employed NBP optical filter, between 7.5 and 7.7 μm. Unlike to PET, it was found that its D_p is around 350 μm indicating that the absorbed and therefore emitted radiation may not be considered on the surface of PE but, in a range close to surface. The relatively high D_p of PE raises another question related to the accuracy of the surface temperature of PE obtained by IR thermography. In other words, the temperature read by the IR camera may correspond to the temperature of the 350 μm thick layer beyond the surface. Hence, it was required to understand how much difference may occur between the actual surface temperature and the recorded temperature by the IR camera. This point was investigated performing another preliminary IR thermography test using a PE plate. Similar to the former preliminary tests done with PET, the plate was heated using the identical IR lamp and the back surface temperature of the PE plate was recorded by the optical filter mounted IR camera and two TCs, namely TC-1 and TC-2. P_{lamp} was changed between 60% and 90% and four different measurements were obtained at four steady state temperatures. In Fig. 8 (a) and (b), the test setup for IR heating of PE plate is presented. As it is shown Fig. 8 (b), the TC-1 and TC-2 were attached in the midpoint and 4 mm away from the lower edge, respectively. A wood-based panel made of medium-density fiberboard (MDF) was used as a barrier and positioned in front the IR lamp. A small frame (70 × 70 mm) was designed for positioning the PE plate. The reason for using a barrier was to perform an IR thermographic measurement on the back surface of the PE plate, without any disturbance of a direct emission from IR lamp to the IR camera. In addition, the front surface of the barrier was covered with metallic adhesive tape in order to limit heating on the barrier, as potential heat transfer from the barrier to the PE plate would cause an erroneous temperature measurement. Furthermore, a transparent adhesive tape was used to fix the position of the attached TCs, as also presented in Fig. 8 (b).

The comparison between the IR thermography and the TC measurements are displayed in Fig. 9 (a) and (b). In Fig. 9 (a), the temperature values recorded by the IR camera and the two TCs at steady state condition are presented. The term -position- in Fig. 9 (a) represents the distance between the endpoints of the axis defined in the vertical direction, as shown Fig. 8 (b). The temperature values recorded by the IR camera were read alongside this axis which was positioned halfway between the right and left edges of the plate, like the TC-1 and TC-2. As it is seen in Fig. 9 (b) the general trend in the ΔT between the TC recordings and the IR thermography was around 1–2 °C, except the two measurements which show difference around 3 °C. Apart from the relatively high D_p of PE, the potential uncertainties on the contact quality between the TCs and the plate during the IR heating may increase the margin of error of measurement, and thus ΔT. Nevertheless, it is assumed that the optical filter mounted IR camera provided surface temperature on PE with a small error, which is mostly less than 2 °C. Considering that the average measured temperature is around 70 °C, it may be stated that the error in the temperature read by IR camera is less than 3%.

The other limitation of the developed experimental methodology at this moment was that the surface temperature measurements could only be done at steady-state conditions. It was observed in all the preliminary IR thermography tests that the externally mounted optical filter causes a potential drift in the UI values registered by the IR detector where the UI values increased over time. Unlike the factory built-in filters that are mounted inside IR cameras, the externally mounted filter is not cooled which eventually may cause a potential self-heating on the filter over time and thus, may cause an additional radiation detected by the IR detector [40]. The two points related to the error in the surface temperature of PE and, the IR thermographic measurements obtained only at steady state temperatures are thus needed to be analyzed further. Nevertheless, the developed experimental methodology

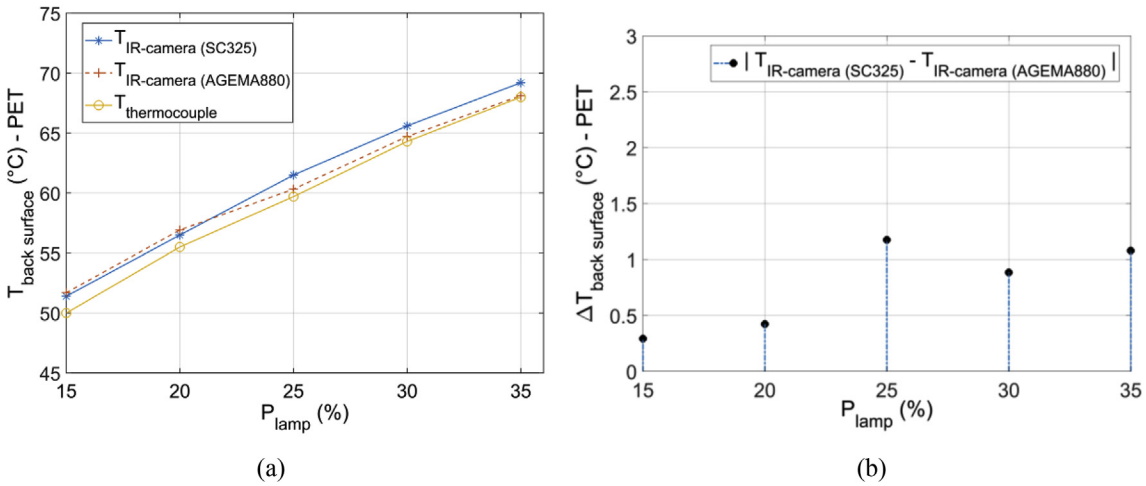

Fig. 7. Preliminary IR thermography tests using PET plate for the sensitivity analyses of the optical filter mounted IR camera (a) and, the measured ΔT between the two IR cameras (b).

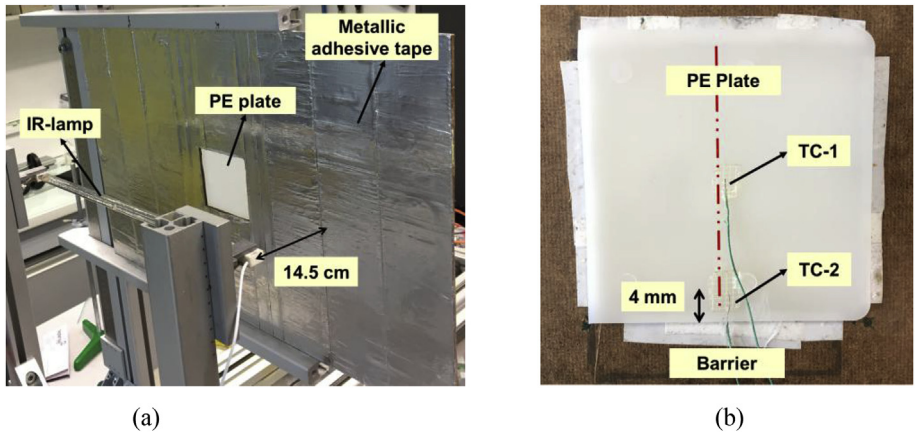

Fig. 8. Test setup for IR heating of PE plate (a) and the positions of the mounted TCs on the back surface (b).

enables to obtain a surface temperature on semi-transparent PE medium that is close enough to the real surface temperature, which may not be obtained using a typical IR camera due to the relatively narrow low-transmittance bands of PE.

4.2. *Experimental – numerical comparisons for IR heating of PE plate*

The comparisons between the predicted and experimentally measured temperatures were done adopting the identical conditions for the case of IR heating of a PE plate. IR heating experiments were carried out

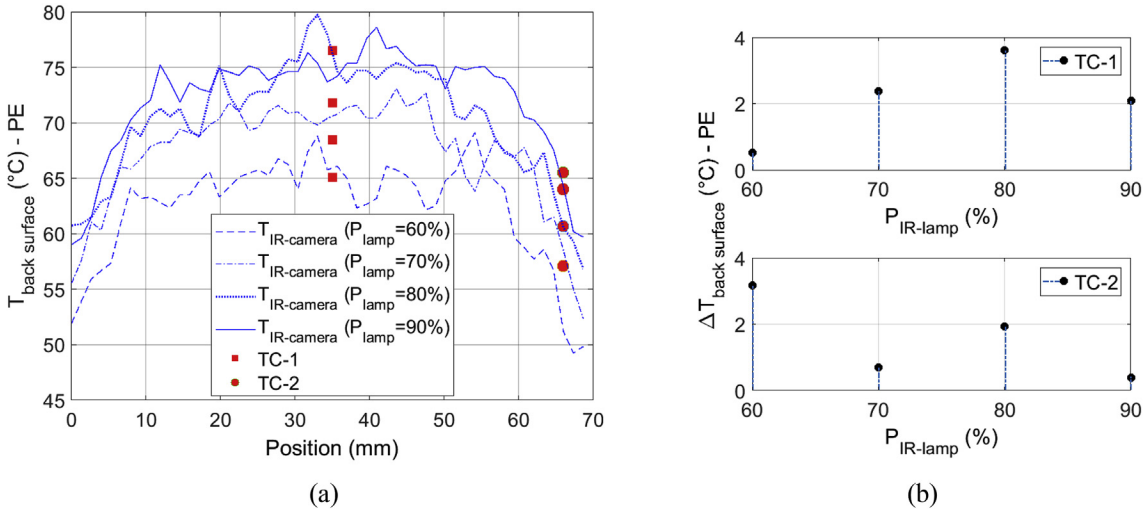

Fig. 9. The comparisons between the temperature fields obtained via IR thermography and the two attached TCs on the vertical direction to the PE plate (a) and, the obtained ΔT at each measurement step (b).

using an identical 2.2 mm thick PE plate tested in the preliminary IR thermography experiments. Similar to the preliminary experiments, the PE plate was heated with the halogen 1 kW IR lamp. Whereas, P_{lamp} was set to 100% of its nominal power, at which the temperature of the IR lamp filament was 2400 K. In order to cross verify the temperature fields obtained from IR thermography, three TCs were attached on the back surface of the PE plate, namely TC-1, TC-2 and TC-3. The TC-1 and TC-2 were positioned 9 mm and 4 mm away from the left and the lower edges of the plate, respectively. TC-3 was attached in the midpoint of the back surface. The IR heating and the TC recordings were started simultaneously so that the real-time temperature evolution of the plate was recorded in three different points for comparing it with the predicted heating behavior obtained from the numerical studies. In addition, it was observed that the back surface temperature reached steady-state after 600 s of heating and the IR thermographic measurements were thus obtained when the temperature of the plate was at steady-state.

The front surface of the PE plate was positioned 8 cm away from the IR lamp. This distance was chosen based on the β_λ (T) behavior of PE and the temperature profile observations obtained from the preliminary IR heating experiments of the PE plate. More specifically, it was aimed to reach a steady-state temperature on the PE plate which is below, but close to its melting range Since the β_λ (T) of PE changes significantly at temperatures close to its melting range (Fig. 4 (a)), a condition at which the polymer is heated up to this range may help to highlight how the temperature dependency in β_λ affects temperature field predictions. Hence numerical-experimental comparisons presented here does not only aim to assess the prediction accuracy of the model including β_λ (T) as numerical input, but also reveals the lack of prediction if a constant β_λ is taken into account in the model, especially for the cases where the polymer is heated up to temperatures close to its melting range. To analyze both the points, a parametric case study was done where two different simulation cases were built (Table 3). In the simulation case-1 (C-1) the absorption characteristics of the PE medium was modeled as independent of temperature adopting only $\nabla.q_r$ (25 °C). In the simulation case-2 (C-2), the computation was done considering the temperature dependent absorption characteristics ($\nabla.q_r$ (T)) computed using the β_λ (T) values (Table 3). For both the cases, all the other boundary conditions were built in exact manner adopting the identical conditions as applied in the IR heating experiments. In the model, the plate geometry was meshed with 2800 linear hexagonal elements, and the temperature of each mesh element was computed as the average temperature of its nodes' temperatures. Based on the experimental time required for reaching the steady-state, heating of the plate was simulated up to 600 s. The emitted radiation from the IR lamp was modeled using 1.5 million rays. This number of ray was chosen regarding the convergence analyses reported by Cosson et al. [35], which run ray tracing computations using RAYHEAT. In terms of computational cost, the ray tracing and $\nabla.q_r$ computations took 10 min for C-1 and 65 min for C-2 using an Intel Core i5 processor (with 2.40 GHz, 8.0 Gb of RAM).

As aforementioned, the transient heat transfer problem combined with conduction and convection, beside of radiation phenomenon, was solved using COMSOL Multiphysics where the iterative closed-loop computations were performed establishing a connection between RAYHEAT and COMSOL Multiphysics® via MATLAB LiveLink. Conduction between the barrier and the PE plate was taken into account including thermal contact resistance (TCR) at the barrier/plate interface. The TCR value at the barrier/plate interface was chosen as 600 W/m^2K from Ref. [41]. In addition, the thermophysical properties of the barrier were adopted from literature. The thermophysical properties of different types of MDF were experimentally analyzed in Refs. [42,43]. Since the MDF type of the barrier used in this study it is not known, the thermophysical properties of MDF found in Refs. [42,43] were averaged and adopted for the barrier. In the model, the C_p, k and ρ of the barrier were defined as 1000 J/kg/K, 0.10 W/m/K and 690 kg/m^3, respectively. It was also assumed that all these adopted parameters are independent of temperature. In addition, potential heat losses due to convection and self-emission of the PE plate were taken into account in the model. The natural convection cooling on the PE plate was modeled using the relation proposed by Churchill and Chu [44] for vertical wall surfaces. In case of IR heating up to 600 s, the momentum of buoyancy-driven air flow over the vertical surfaces of the plate was also considered. At very first step, the regime of the buoyancy-driven heated air flow was estimated calculating the Grashof Number [45]. It was found that the laminar flow can be assumed, regarding the geometrical dimensions of the PE plate and, the maximum and minimum temperatures of the plate surface. Considering the identical case used in the IR heating experiments and assuming a laminar flow for air, the heat transfer coefficient (h (W/m^2K)) was computed in COMSOL considering the front and back surfaces of the plate and, used as input in the iterative closed-loop computations. Due to varying convective velocity field of air alongside of the front and back surfaces of the plate, the computed h values on both the surfaces were found between 5 and 9 W/m^2K.

The self-emission was also modeled on both front and back vertical surfaces of the PE plate. Using the $T_\lambda^{i,\cap}$ (97 °C) and $R_\lambda^{i,\cap}$ (97 °C) measurements of the thinnest PE film used in this study (250 μm thick samples), the emissivity of PE was calculated around 0.77. The measurements at this temperature step were chosen considering that the polymer was heated up to 130 °C for forming processes. It should be pointed out here that, in the finite element modeling (FEM) software, emissivity is modeled on the surface considering a case of opaque materials which is parametrized as surface emissivity ($\varepsilon_{surface}$). Therefore, it is assumed that all incident radiation is either absorbed or reflected on the surface of opaque medium, whereas no transmission of radiation through its medium is considered. However, this is not the case for PE polymer as it is semi-transparent [37,38,46], which is also shown in this study considering its spectroscopic measurements. Simply, the emissivity of semi-transparent materials is a global physical quantity which theoretically represent emission from medium but not from surface [20,47], due to volumetric absorption. In other words, the emitted energy, and thus the value of emissivity, of an opaque material does not change by a change in their thickness, conversely it is strongly affected by a change in the thickness of semi-transparent materials [48] which makes $\varepsilon_{surface}$ fundamentally unsound. Nevertheless, it may be assumed that the emissivity measurements in very thin PE samples may represent $\varepsilon_{surface}$. For instance, the optical properties of 100 μm thick HDPE and LDPE films was experimentally characterized by Okada et al. [37] and the emissivity values for both type of PE polymer was found around 0.28. The transmittance spectra and absorption bands of both the studied PE polymers in Ref. [37] show close agreement with the spectroscopic analyses of PE samples studied here. Similarly, the reflectance and transmittance characteristics of 100 μm thick HDPE film was reported by Mastai et al. [46] which also show close agreements with [37]. In addition, following Equations (1) and (2), and knowing that $A_\lambda = f(\rho_\lambda, \tau_\lambda)$ and $\tau_\lambda = f(\beta_\lambda, x)$, the determined values of ρ_λ and

Table 3
Case studies adopted for numerical simulations.

	Radiation absorption in polymer medium
Simulation Case - 1 (C-1)	Constant radiation absorption with $\nabla.qr$ (25 °C)
Simulation Case - 2 (C-2)	Temperature-dependent radiation absorption with $\nabla.q_r$ [T,x,y,z]) between 25 and 128 °C

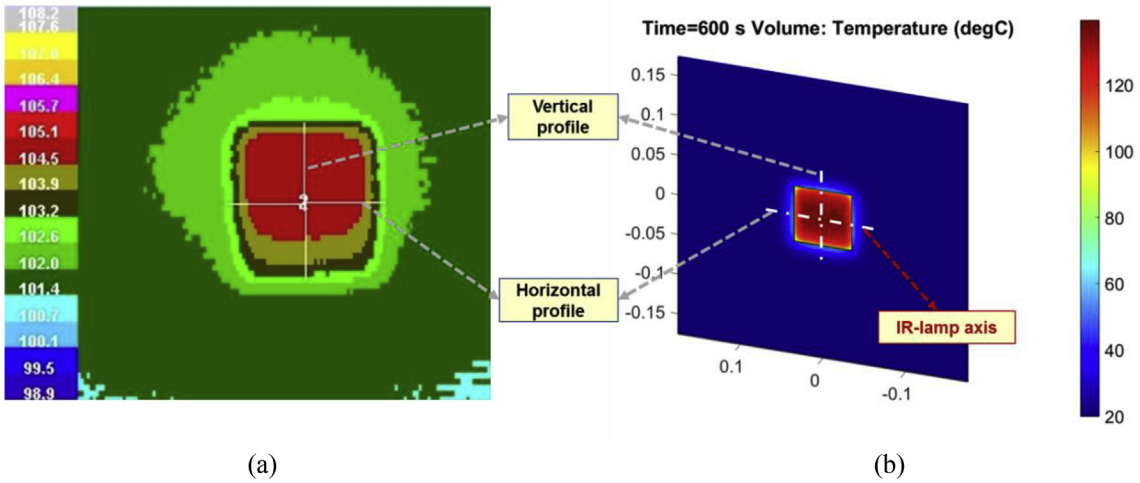

Fig. 10. Temperature field comparisons on the identically-created vertical and horizontal profiles on both the IR thermography (a) and numerical simulation (b) of the PE plate.

β_λ from our spectroscopic measurements were used for calculating A_λ of a 100 μm thick PE medium. The comparison between the calculated A_λ and the absorbance spectrum of HDPE and LDPE in Ref. [37] also showed close agreement. Therefore, the emissivity value of 100 μm thick PE proposed in Ref. [37] was assumed as $\varepsilon_{surface}$ in the model, instead of adopting emissivity value of the 250 μm thick PE sample that was used in this study.

For the numerical - experimental comparisons; two profiles were defined in vertical and horizontal directions on the PE plate. The horizontal profile was defined alongside the IR lamp axis whereas the vertical profile was perpendicular to the IR lamps axis. In Fig. 10, identically-created profiles on both IR thermography of the plate (a) and, the numerical simulation (b) are presented. The scale bar on the IR thermography of the plate (Fig. 10 (a)) represents the radiometric values (UI).

In Fig. 11, the comparisons between the temperature profiles obtained from the experimental and the numerical studies are presented on the vertical (a) and horizontal (b) profiles. As it is seen, C-2 predicts the back surface temperature of the PE plate closely, whereas C-1 overestimates the experimental results by around 10 °C. In terms of accuracy of the model built as C-2, two different points may be raised further. First of all, ΔT between the predicted and experimentally measured temperature is less than 3 °C throughout the vertical profile. Whereas, in terms of comparisons on the horizontal profile, this small difference is only seen on the middle zone of the plate (the position between 10 and 60 mm, which is defined in x axis). In addition to this, ΔT on the horizontal profile becomes somewhat significant considering the zones close to the edge of the plate which may be attributed to the underestimation of the potential conduction heat losses between the barrier and PE plate. As aforementioned, the thermophysical properties of the wood-based barrier were adopted from literature, but not experimentally characterized. Secondly, such difference does not exist on the vertical profile where also a non-balanced temperature distribution alongside the vertical direction of the plate is seen, as illustrated in Fig. 11 (a). The non-balanced profile is induced by the heated air that moves upward along the heated vertical surface. The close prediction then shows that the computed h which considers the buoyancy-driven air flow in the vertical direction, was well defined. This may also be the dominating mode of heat transfer on the vertical direction, rather than conduction between the barrier and the plate, and thus results in better convergence between the predicted and experimental results on the vertical profile. Considering that the thermoforming window of semi-crystalline PE is around 4–5 °C, the ΔT between the experimental results and both the predicted values of C-1 and C-2 clearly indicates that characterization of the temperature-dependent thermo-optical properties of semi-crystalline polymers may be one of the key factors for the accuracy in temperature field predictions.

The real-time temperature evolution on the PE plate was also analyzed comparing the TC recordings to the numerical results obtained from C-2. The numerical results were taken at the same location of the TC-3, which was attached at the midpoint of the back surface. In both the TC-1 and TC-2 measurements, the fluctuations were seen which was probably due to contact quality between the TC and the PE plate, in contrast to the TC-3 measurements. In this drawback, the contact quality is deteriorated not only due to securing a fixed position for the TC but also the softening behavior of the PE polymer, especially seen when it is close the melting range. Therefore, it may be stated that the non-invasive IR thermography may provide more reliable temperature

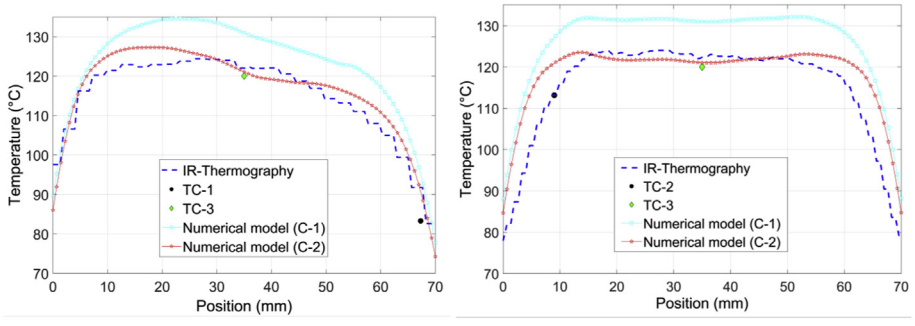

Fig. 11. The predicted and measured steady state temperature profiles on the vertical (a) and horizontal profiles (b), defined on the PE plate's back surface.

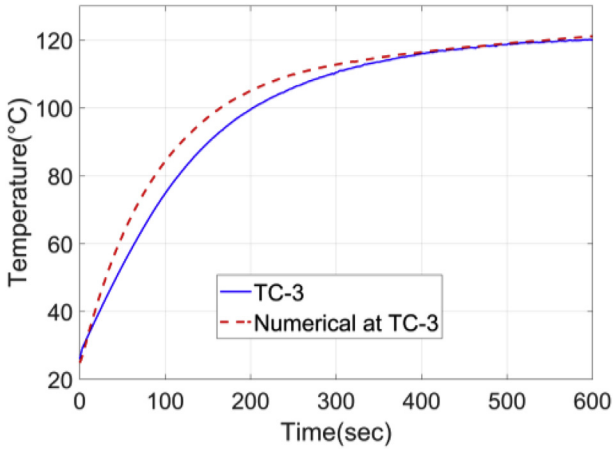

Fig. 12. Experimental and numerical (C-2) comparisons on the midpoint of the PE plate's back surface, considering the real-time temperature evolutions until reaching steady state.

measurements that can also be a reference for the numerical-experimental comparisons. Nonetheless, since no such fluctuations was observed in the TC-3 measurements, the comparison between the precited real-time temperature evolution to the TC-3 recordings was presented in Fig. 12. Furthermore, in terms of comparisons between the TCs and the predicted temperature, the position of the TC-3 may be the most reliable to analyze the accuracy of the temperature-dependent numerical model with respect to the absorbed radiation. As illustrated in Fig. 12, the temperature evolution was closely predicted, especially at the steady state temperature zone. Regarding the entire time range up to 600 s, ΔT between the experimental and numerical values may not be fully negligible in the temperature ramp-up period, where after the ΔT reduces to 1 °C at the steady state zone. Using the current IR heating test setup configurations, C-2 may still need to be optimized in terms of accuracy in the numerical inputs, other than thermal radiation parameters of the heated polymer. However, it should be mentioned here that, the IR heating experiments carried out in this study are the pilot analyses for the thermoforming process of PE polymer. More specifically, in the thermoforming process of PE studied here, thermal radiation is the dominant mode of heat transfer where no barrier is used around a polymer with shorter heating time duration than the one adopted here.

5. Conclusions

In this study, an experimental methodology and numerical approach is proposed for radiation heat transfer in semi-crystalline thermoplastics. The proposed experimental and numerical approaches were analyzed here for the case of IR heating of PE. The challenges for radiation transport in semi-crystalline polymers may be categorized into the two main aspects: optical heterogeneity in polymer medium due to semi-crystalline nature and, semi-transparency in certain type of semi-crystalline polymers, such as PE analyzed here. Considering any type of monochromatic or polychromatic radiation source - such as laser and Light Emitting Diodes (LED) - the combined experimental-numerical approach proposed in this study may be adopted for temperature field predictions and non-invasive temperature measurements for the radiatively heated semi-crystalline thermoplastics.

Optical scattering is inherent for any type of semi-crystalline polymer due to their semi-crystalline nature, at which it especially becomes a key in a case that the polymer is also semi-transparent regarding the spectral range of IR radiation. The radiation heat transfer model presented in this study proposes a macroscopic numerical approach to address indirectly the optical scattering and the change in its behavior under heating condition, without modeling how the light scatters inside of polymer medium. In other words, the effect of optical scattering on the absorption characteristics of semi-crystalline PE was taken into account without modeling the spatial distribution of the scattered light intensity at microscopic levels, which offers computationally cost-effective numerical solutions. To model this relation under varying temperature, an experimental methodology was developed. Initially, the optical measurement method, particularly for the transmittance characteristics of semi-crystalline PE, was discussed and its effect on the accuracy of the numerical input was highlighted. The directional-hemispherical optical characteristics of PE were determined under heating and, its temperature-dependent behavior was demonstrated especially in the temperature ranges close to the melting range which is strongly related to the change in its crystalline phase. Thanks to the experimental analyses, β_λ (T) values of PE were calculated between room temperature up to 128 °C and used as numerical inputs in the model. Thanks to the closed-loop iterative computation algorithm built in the model, the temperature dependence in the absorption characteristics was modeled at mesh scale.

The accuracy of the model was assessed performing numerical-experimental comparisons for the case of IR heating of PE plate. Temperature fields and evolutions on the PE plate was measured via TCs and IR thermography Due to the semi-transparent medium of PE, an experimental methodology was developed for obtaining the most accurate surface temperature possible via IR thermography. Based on the successive preliminary IR thermography tests, it was observed that IR thermography of PE may be obtained with a maximum uncertainty up to 2 °C. A parametric case study was performed adopting the two different simulation cases (C-1 and C-2) with the aim of analyzing the effect of temperature dependent optical properties on the temperature field predictions of radiatively heated PE. The C-2, which was built using β_λ (T), predicted the temperature closely where the difference between the experimental and numerical results was less than 3 °C in the middle zone of the PE plate. Conversely, the C-1 overestimated the experimental results by around 10 °C which is likely happen due to the ignorance of the weakening in the absorption characteristics of PE induced by β_λ (T). Even though the predicted temperature shows somewhat difference close to the edges of the PE plate, the close prediction in the middle zone of the plate demonstrates the accuracy on the computation of the absorbed radiation in PE medium which evolves under varying temperature due to β_λ (T). Considering that the thermoforming window of semi-crystalline PE is around 4–5 °C which lie in polymer's melting range, its temperature-dependent thermo-optical properties may be one of the key factors for the accuracy in temperature field predictions.

In order to validate the model further, thermal measurements may be extended including through-thickness temperature profiles of a heated sample in more complex geometries other than a square or a rectangular slab. However extra attention may be given to the radiation transport in such condition, as the complexity in ray tracing modeling may also increase due to combined effect of both the higher geometrical details and optical scattering phenomenon. In future work, a numerical model at microscopic level will be developed, that also addresses the spatial distribution of the scattered light which may be a function of the size of scatterer in relation to the crystalline morphology of semi-crystalline polymers. Thanks to this, a complete solution for the absorbed radiation in an optically heterogeneous 3D polymer medium may be obtained.

Acknowledgment

The authors gratefully acknowledge the financial support of Procter & Gamble Co. for this research project.

Special thanks to Mr. Christophe Escape of Procédés, Matériaux et Energie Solaire (PROMES) - CNRS laboratory for his technical support and assistance with the spectroscopic tests performed in this research.

References

[1] R. Klein, Laser Welding of Plastics: Materials, Processes and Industrial Applications, Wiley-VCH Verlag GmbH & Co. KGaA, Weinheim, Germany, 2011http://doi.wiley.com/10.1002/9783527636969.

[2] Burkhardt Gert, Hüsgen Ulrich, Kalwa Matthias, Pötsch Gerhard, Schwenzer Claus, Plastics Processing, 1. Processing of thermoplastics, Ullmanns Encycl Ind Chem (2011), https://doi.org/10.1002/14356007.a20_663.pub2.

[3] X.F. Xu, A. Parkinson, P.J. Bates, G. Zak, Effect of part thickness, glass fiber and crystallinity on light scattering during laser transmission welding of thermoplastics, Optic Laser Technol 75 (2015) 123–131, https://doi.org/10.1016/j.optlastec.2015.06.026.

[4] A. Denis, E. Dargent, P.H. Lebaudy, J. Grenet, C. Vautier, Dependence on the spectral scattering coefficient on crystallinity into semicrystalline polyester, J Appl Polym Sci 62 (1996) 1211–1218, https://doi.org/10.1002/(SICI)1097-4628(19961121)62:8<1211::AID-APP11>3.0.CO;2-A.

[5] S. Boztepe, R. Gilblas, O. de Almeida, C. Gerlach, Y. Le Maoult, F. Schmidt, The role of microcrystalline structure on optical scattering characteristics of semi-crystalline thermoplastics and the accuracy of numerical input for IR heating modeling, Int J Material Form (2017), https://doi.org/10.1007/s12289-017-1386-z.

[6] D. Hakoume, L.A. Dombrovsky, D. Delaunay, B. Rousseau, Spectroscopic diagnostics of morphological changes arising in thermal processing of polypropylene, Appl Opt 53 (2014) 2702, https://doi.org/10.1364/AO.53.002702.

[7] B. Heck, T. Kawai, G. Strobl, Time dependent light attenuation measurements used in studies of the kinetics of polymer crystallization, Polymer 47 (2006) 5538–5543, https://doi.org/10.1016/j.polymer.2005.11.098.

[8] R. Apetz, M.P.B. Bruggen, Transparent alumina: a light-scattering model, J Am Ceram Soc 86 (2003) 480–486, https://doi.org/10.1111/j.1151-2916.2003.tb03325.x.

[9] M. Ilie, J.-C. Kneip, S. Matteï, A. Nichici, C. Roze, T. Girasole, Laser beam scattering effects in non-absorbent inhomogenous polymers, Optic Laser Eng 45 (2007) 405–412, https://doi.org/10.1016/j.optlaseng.2006.07.004.

[10] E. Berrocal, D.L. Sedarsky, M.E. Paciaroni, I.V. Meglinski, M.A. Linne, Laser light scattering in turbid media Part I: experimental and simulated results for the spatial intensity distribution, Optic Express 15 (2007) 10649–10665, https://doi.org/10.1364/OE.15.010649.

[11] A. Humphrey, T. Harman, M. Berzins, P. Smith, A scalable algorithm for radiative heat transfer using reverse Monte Carlo ray tracing, Int. Conf. High Perform. Comput, Springer, 2015, pp. 212–230.

[12] D.V. Tsu, M. Muehle, M. Becker, T. Schuelke, J. Slagter, Quantification of diffuse scattering in glass and polymers by parametric power law analysis of UV to NIR light, Surf Coating Technol. (2017), https://doi.org/10.1016/j.surfcoat.2017.08.054.

[13] R. BerndKeller, W.-N. Su, P. Eyerer, Temperature Dependent Optical Properties of Polymers as a Basis for Laser Process Modeling, (n.d.).

[14] F. Becker, H. Potente, A step towards understanding the heating phase of laser transmission welding in polymers, Polym Eng Sci 42 (2002) 365–374.

[15] M. Devrient, X. Da, T. Frick, M. Schmidt, Experimental and simulative investigation of laser transmission welding under consideration of scattering, Phys Procedia 39 (2012) 117–127, https://doi.org/10.1016/j.phpro.2012.10.021.

[16] S. Boztepe, R. Gilblas, O. De Almeida, F. Schmidt, Y. Le Maoult, The role of microcrystalline structure on the temperature-dependent thermo-optical properties of semi-crystalline thermoplastics and non-invasive temperature measurements, SFT 2017-Congrès Annu. Société Fr. Therm, 2017.

[17] B. Wunderlich, Thermal Analysis of Polymeric Materials, Springer, Berlin, 2005.

[18] G.H. Michler, Electron microscopic investigations of morphology and structure formation of polymers, J Macromol Sci Part B 35 (1996) 329–355, https://doi.org/10.1080/00222349608220384.

[19] A.J. Peacock, Handbook of Polyethylene: Structures, Properties, and Applications, Marcel Dekker, New York, 2000.

[20] Y. Le Maoult, F. Schmidt, Infrared radiation applied to polymer processes, in: N. Boyard (Ed.), Heat Transf. Polym. Compos. Mater. John Wiley & Sons, Inc., 2016, pp. 385–423 http://onlinelibrary.wiley.com/doi/10.1002/9781119116288.ch13/summary , Accessed date: 18 December 2016.

[21] S. Monteix, Y.L. Maoult, F. Schmidt, J.P. Arcens, Quantitative infrared thermography applied to blow moulding process: measurement of a heat transfer coefficient, Quant InfraRed Thermogr J 1 (2004) 133–150, https://doi.org/10.3166/qirt.1.133-150.

[22] J.R. Howell, M.P. Menguc, R. Siegel, Thermal Radiation Heat Transfer, sixth ed., CRC Press, 2015.

[23] M.F. Modest, Radiative Heat Transfer, second ed.2 edition, Academic Press, Amsterdam ; Boston, 2003.

[24] J. Manara, M. Arduini-Schuster, L. Hanssen, Integrating sphere reflectance and transmittance intercomparison measurements for evaluating the accuracies of the achieved results, High Temp - High Press 38 (2009) 259–276.

[25] N. Billon, V. Henaff, E. Pelous, J.M. Haudin, Transcrystallinity effects in high-density polyethylene. I. Experimental observations in differential scanning calorimetry analysis, J Appl Polym Sci 86 (2002) 725–733, https://doi.org/10.1002/app.10982.

[26] S. Boztepe, A. Thiam, O. de Almeida, Y. Le Maoult, F. Schmidt, Experimental Analysis on the Coupled Effect between Thermo--optical Properties and Microstructure of Semi--crystalline Thermoplastics, in: n.d.

[27] A.C.A. Asséko, B. Cosson, F. Schmidt, Y.L. Maoult, E. Lafranche, Laser transmission welding of composites-Part A: thermo-physical and optical characterization of materials, Infrared Phys Technol 72 (2015) 293–299, https://doi.org/10.1016/j.infrared.2015.02.004.

[28] C.L. Choy, Thermal conductivity of polymers, Polymer 18 (1977) 984–1004.

[29] K. Kurabayashi, Anisotropic thermal properties of solid polymers, Int J Thermophys 22 (2001) 277–288.

[30] G. Höhne, W. Hemminger, H.-J. Flammersheim, Differential Scanning Calorimetry: an Introduction for Practitioners, Springer-Verlag, Berlin; New York, 1996http://public.eblib.com/choice/publicfullrecord.aspx?p=3098843 , Accessed date: 9 April 2018.

[31] W. Glenz, N. Morosoff, A. Peterlin, Density of drawn polyethylene, J Polym Sci C Polym Lett 9 (1971) 211–217.

[32] I. Perepechko, Low-Temperature Properties of Polymers, Elsevier, 2013.

[33] N.S. Yenikolopyan, L.N. Raspopov, A.D. Pomogailo, F.A. Khrisostomov, A.M. Bochkin, V.V. Filippov, V.G. Nikol'skii, Structure and density of the amorphous and crystalline phases in low-density linear polyethylenes, Polym Sci USSR 31 (1989) 2882–2891, https://doi.org/10.1016/0032-3950(89)90327-4.

[34] U.W. Gedde, A. Mattozzi, Polyethylene morphology, in: A.-C. Albertsson (Ed.), Long Term Prop. Polyolefins, Springer Berlin Heidelberg, Berlin, Heidelberg, 2004, pp. 29–74, , https://doi.org/10.1007/b94176.

[35] B. Cosson, F. Schmidt, Y. Le Maoult, M. Bordival, Infrared heating stage simulation of semi-transparent media (PET) using ray tracing method, Int J Material Form 4 (2011) 1, https://doi.org/10.1007/s12289-010-0985-8.

[36] P. Vueghs, H.P. de Koning, O. Pin, P. Beckers, Use of geometry in finite element thermal radiation combined with ray tracing, J Comput Appl Math 234 (2010) 2319–2326, https://doi.org/10.1016/j.cam.2009.08.088.

[37] T. Okada, R. Ishige, S. Ando, Analysis of thermal radiation properties of polyimide and polymeric materials based on atr-ir spectroscopy, J Photopolym Sci Technol 29 (2016) 251–254.

[38] P.T. Tsilingiris, Comparative evaluation of the infrared transmission of polymer films, Energy Convers Manag 44 (2003) 2839–2856, https://doi.org/10.1016/S0196-8904(03)00066-9.

[39] S. Boztepe, R. Gilblas, O. de Almeida, Y. Le Maoult, F. Schmidt, A Non-invasive Experimental Approach for Surface Temperature Measurements on Semi-crystalline Thermoplastics, 2017, p. 060007, , https://doi.org/10.1063/1.5008070.

[40] M. Vollmer, K.-P. Mallmann, Infrared Thermal Imaging: Fundamentals, Research and Applications, John Wiley & Sons, 2017.

[41] M. Bordival, Modélisation et optimisation numérique de l'étape de chauffage infrarouge pour la fabrication de bouteilles en PET par injection-soufflage, ENMP, Paris, 2009http://www.theses.fr/2009ENMP1647 , Accessed date: 10 July 2018.

[42] T. Kawasaki, S. Kawai, Thermal insulation properties of wood-based sandwich panel for use as structural insulated walls and floors, J Wood Sci 52 (2006) 75–83, https://doi.org/10.1007/s10086-005-0720-0.

[43] K.Y. Li, C.M. Fleischmann, M.J. Spearpoint, Determining thermal physical properties of pyrolyzing New Zealand medium density fibreboard (MDF), Chem Eng Sci 95 (2013) 211–220, https://doi.org/10.1016/j.ces.2013.03.019.

[44] S.W. Churchill, H.H.S. Chu, Correlating equations for laminar and turbulent free convection from a vertical plate, Int J Heat Mass Transf 18 (1975) 1323–1329, https://doi.org/10.1016/0017-9310(75)90243-4.

[45] F.P. Incropera, F.P. Incropera (Eds.), Fundamentals of Heat and Mass Transfer, sixth ed., John Wiley, Hoboken, NJ, 2007.

[46] Y. Mastai, Y. Diamant, S.T. Aruna, A. Zaban, TiO2 nanocrystalline pigmented polyethylene foils for radiative cooling applications: synthesis and characterization, Langmuir 17 (2001) 7118–7123.

[47] G.-Y. Lai, J.X. Rietveld, Role of polymer transparency and temperature gradients in the quantitative measurement of process stream temperatures during injection molding via IR pyrometry, Polym Eng Sci 36 (1996) 1755–1768.

[48] R. Gardon, The emissivity of transparent materials, J Am Ceram Soc 39 (1956) 278–285.